Experimental and Numerical Simulation of Corrosion Behavior of A333 Carbon Steel Weldment in CO_2-Saturated Environment

Taiwo Onaopemipo Alao
Department of Mechanical Engineering, Universiti Teknologi PETRONAS, Bander Seri Iskandar, 32160, Perak, Malaysia
taiwo_22012044@utp.edu.my

K. E. Kee
Department of Mechanical Engineering, Universiti Teknologi PETRONAS, Bander Seri Iskandar, 32160, Perak, Malaysia
keekokeng@utp.edu.my (corresponding author)

Mazli Mustapha
Department of Mechanical Engineering, Universiti Teknologi PETRONAS, Bander Seri Iskandar, 32160, Perak, Malaysia
mazli.mustapha@utp.edu.my

Kehinde Temitope Alao
Department of Mechanical Engineering, Universiti Teknologi PETRONAS, Bander Seri Iskandar, 32160, Perak, Malaysia
kehinde_22012050@utp.edu.my

Received: 31 July 2025 | Revised: 5 September 2025 and 22 September 2025 | Accepted: 24 September 2025

 DOI: https://doi.org/10.48084/etasr.13539

ABSTRACT

The galvanic corrosion behavior of A333 carbon steel weldments in carbon dioxide gas-bubbled 3 wt% NaCl solution was studied in the current research by experimental electrochemical measurements and computational modeling. Zero Resistance Ammeter (ZRA) measurements were employed to quantify the galvanic corrosion rates of Parent Metal (PM), Heat-Affected Zone (HAZ), and Weld Metal (WM) at temperatures of 25 °C and 60 °C for homogeneous and heterogeneous welds. These experimental results were compared with computational simulations using COMSOL Multiphysics version 5.6, where the Nernst-Planck and Tafel equations were applied to simulate them. The findings revealed that galvanic interactions between the weldment zones increased with temperature, with the HAZ exhibiting the highest corrosion rate and behaving anodically due to electrochemical potential variation and microstructural differences at both temperatures. The comparison between experimental and simulated corrosion rates demonstrated good agreement, confirming the predictive capability of the model with the heterogeneous weld being more susceptible to galvanic corrosion than the homogeneous weld. This study offers valuable insights into the impact of temperature on galvanic corrosion, and the significance of using simulation tools in predicting galvanic corrosion between the weldment zones.

Keywords- weld corrosion; galvanic corrosion; numerical simulation; COMSOL Multiphysics

I. INTRODUCTION

Internal corrosion is a major integrity threat to oil and gas pipeline systems, particularly in carbon steel infrastructure which is exposed to aggressive environments. It arises mainly from the electrochemical reactions between pipeline materials and carried fluids that contain carbon dioxide (CO_2), hydrogen sulfide (H_2S), water, and dissolved salts [1, 2]. Weldments, which are prone to local microstructure and chemical composition changes caused by welding thermal cycles, lead to the formation of galvanic cells between the PM, HAZ, and WM [3, 4]. The presence of carbon dioxide worsens the localized corrosion through the formation of carbonic acid in moisture-condensing conditions, and operating conditions, such

as flow turbulence, temperature gradients, and solution pH, enhance degradation at weld interfaces [5]. These effects, if not checked, can result in preferential weld corrosion, decrease service life, and induce premature pipeline failure [6].

The microstructural disparity among the PM, HAZ, and WM plays a significant role in galvanic corrosion behavior of weldments. Specifically, PM, which mainly consists of ferrite and pearlite, presents lower corrosion rates due to its stable microstructure [7, 8]. In contrast, HAZ, which involves a combination of coarse and fine grains, is more susceptible to corrosion due to phase disparity and increased hardness [9]. Furthermore, WM, consisting of phases, such as delta ferrite and sigma, can exhibit anodic behavior in galvanic couples which accelerate their corrosion rate relative to the adjacent zones [10]. The potential difference between PM, HAZ, and WM can cause galvanic corrosion, with HAZ and WM exhibiting higher corrosion rates, particularly in the presence of chloride ions and higher temperatures [11]. The heat input during welding affects the microstructure, which results in coarser grains and higher susceptibility of the HAZ to corrosion attack [12]. In general, the knowledge of these microstructural effects is necessary to prevent corrosion in welded joints exposed to aggressive media.

Carbon steel, which is widely used in low-temperature operating conditions, is susceptible to corrosion in CO_2-containing environments. Under these conditions, steel usually develops a protective $FeCO_3$ layer. However, this layer is not uniform, causing localized corrosion, especially when the $FeCO_3$ layer is incomplete or damaged [13]. At high temperatures, the formation of $FeCO_3$ is damaged, which increases the weldment surface susceptibility to corrosion, while lower temperatures enhance its protective quality, with decreased corrosion rates [14]. The presence of H_2S makes the situation more complicated by depositing iron sulfide (FeS) layers, which can either protect the steel or cause further corrosion, depending on the operating environmental conditions [15, 16].

This work presents a new approach that integrates experimental electrochemical methods and numerical simulations for studying the galvanic corrosion behavior of weldments of A333 carbon steel in CO_2-saturated media.

II. MATERIALS AND METHODS

A. Materials

The material used in this study was A333 Grade 6 carbon steel, which is widely employed in low-temperature operational conditions. Weldment samples were extracted from a welded A333 carbon steel pipe spool obtained from an oil field. The material surface was machined to the required pipe thickness and delicately divided into three different sections: PM, HAZ, and WM, following the ASTM A765/A765M standard.

Two types of welding were utilized in the experiments: homogeneous (matching filler metal and base metal composition) and heterogeneous (nickel-containing filler metal). The PM, HAZ, and WM were machined into circular and rectangular shapes, with surface areas of 0.30 cm^2, 0.19 cm^2, and 0.21 cm^2, respectively. These segments were connected with copper wire and flush-mounted in epoxy resin, forming a ready-to-use coupon for electrochemical analysis. The elemental compositions of homogeneous and heterogeneous weldments, determined by Energy Dispersive X-ray Spectroscopy (EDX), are presented in Table I.

TABLE I. EDX RESULTS FOR ASTM A333 GRADE 6 WELDMENTS (HOMOGENEOUS AND HETEROGENEOUS)

Weld type	Section	Mn	S	Si	P	Al	Ni	Fe
Homogeneous	PM	0.8	0.2	0.6	0.2	0.2	0	Bal
	HAZ	0.7	0.0	0.8	0.1	0.1	0	Bal
	WM	0.3	0.0	0.4	0.0	0.3	0	Bal
Heterogeneous	PM	0.9	0.0	0.6	0.2	0.1	0	Bal
	HAZ	0.5	0.1	0.7	0.1	0.4	0	Bal
	WM	0.5	0.0	0.1	0.0	0.3	0.7	Bal

B. Surface Preparation

To achieve proper surface finishes, the samples were ground and polished using sandpapers of varying grit sizes: 60, 120, 240, 320, -grit, and 600. The samples were then polished with diamond suspension for a finer finish. To eliminate any contaminants introduced during machining, the surfaces were cleaned with acetone and dried using hot air. Additionally, a cross-sectional cut of the unsegmented weldment was mounted in epoxy resin as a surface morphology coupon and etched with 2% Nital to reveal the distinct microstructural gradient across the PM, HAZ, and WM regions.

C. Solution Preparation

The chloride-containing solution was prepared by dissolving 3 wt% sodium chloride (NaCl) from Sigma-Aldrich in 1 L glass cells filled with distilled water. The solution was stirred and heated on a hot plate to ensure the complete dissolution of NaCl. To mitigate the dissolved oxygen, the solution was purged with CO_2 for 40 min and continued to be purged throughout the experiment.

D. Electrochemical Measurements

The Zero-Resistance Ammeter (ZRA) test was conducted in a 1 L glass cell to measure the galvanic corrosion rates of the samples at two temperatures: 25 °C and 60 °C. A five-electrode system was employed, with a silver/silver chloride (Ag/AgCl) reference electrode, a platinum counter electrode, and the weldment sample as the working electrode. All electrodes were connected to a potentiostat (ACM Instrument Gill 12 weld tester). Measurements were recorded every min over a 48-h period.

E. Numerical Modeling

To predict the corrosion behavior and mechanisms, the Finite Element Method (FEM) was employed to simulate the current density distribution, ion migration, and diffusion between the weldment surface and the electrolyte solution. COMSOL Multiphysics version 5.6 was used to solve the Partial Differential Equations (PDEs) governing the electrochemical interactions.

The parameters used for numerical simulation, including electrolyte species and their charges, diffusion coefficients, and other key values, are presented in Table II, while the simulated

parameters for the FEM are provided in Table III. These outputs were then used to predict the galvanic corrosion rate.

TABLE II. PARAMETERS FOR ELECTROLYTE SPECIES, CHARGES, AND DIFFUSION COEFFICIENTS

Species (*i*)	Species charges (*Zi*)	Diffusion coefficient (m^2/s) × 10^9
H^+	+1	1.9 [17]
OH^-	-1	5.26 [18]
Fe^{2+}	+2	0.72 [18]
Na^+	+2	1.33 [18]
CO_3	-2	0.92 [18]
Cl^-	-1	2.03 [18]

TABLE III. FEM SIMULATED PARAMETERS

Parameter	Description	Values
cCO_3^{2-}	Initial concentration of CO_3^{2-}	0.086002 mol/m^3
$cHCO_3^-$	Initial concentration of HCO_3^-	0.1237 mol/m^3
cFe^{2+}	Initial concentration of Fe^{2+}	0 mol/m^3
cNa^+	Initial concentration of Na^+	30 mol/m^3
cCl^-	Initial concentration of Cl^-	30 mol/m^3
$E_{eq.cath}$	Equilibrium potential for cathode	-0.58 V
$E_{eq.ano.}$	Equilibrium potential for anode	-0.684 V
$i_{o_}$cath.	Exchange current density (cathode)	100 A/m^2
$i_{o_}$ano.	Exchange current density (anode)	100 A/m^2
α_a	Anodic transfer coefficient	0.5
α_c	Cathodic transfer coefficient	0.5
b_{H+}	Tafel slope for H^+ reduction	0.118 V
b_{Fe2+}	Tafel slope for Fe^{2+} reduction	0.04 V

F. Governing Equations

The Nernst-Planck equation was utilized to model the ion transport and mobility in the electrolyte. After modifications, the equation considered diffusion, migration, and convection, and was written as:

$$N_i = -D\nabla C_i - Z_i F U_i C_i \nabla\phi + C_i V \quad (1)$$

where N_i is known as the flux vector in mol/m^2s, D is the diffusion coefficient in m^2/s, C_i is the concentration of the species i in mol/dm^3, Z_i is the mobility of the species i, which is dimensionless, F is Faraday's constant, U_i is the ionic mobility in mol s/kg, ϕ is the electric potential in Volt, and V is the solvent velocity in m/s.

Assuming an electroneutral, well-mixed, and incompressible electrolyte, (1) was simplified as:

$$\frac{\partial C_t}{\partial t} = -\nabla . N_i = D_i\nabla^2 - Z_i F U_i \nabla . (C_i \nabla\emptyset) . \nabla . (C_i V) \quad (2)$$

The corrosion rate (C_R) is determined using Faraday's law:

$$C_R = \frac{M}{zF\rho} j_{couple} \quad (3)$$

where C_R is the corrosion rate of the corroding section of the galvanic couple in m/s, M is the atomic mass in g/mol, z is the electron number, F is the Faraday's constant in C/mol, ρ is the density of the corroding section of the galvanic couple in kg/m^3, and j couple is the current density in A/m^2.

The Tafel equation was employed to model the electrochemical reactions, relating the current density to the overpotential:

$$\nabla V = A \times In\left(\frac{i}{i_0}\right) \quad (4)$$

where ∇V is the overpotential in Volt, A is known as Tafel slope, i_0 is the exchange current in A/m^2, and i is the current density.

G. Model Description and Boundary Conditions

The FEM model was configured in 2D geometry, with an electrolyte conductivity of 2.5 S/m. To simulate the corrosion rate, a tertiary current distribution interface was employed, with a time-dependent preselection, applying the transporting electrolyte-electrode boundary interface terminals for the three surfaces of the electrodes. The Arbitrary Lagrangian-Eulerian (ALE) approach was used to represent the dynamic interface throughout the corrosion process, with moving mesh techniques considered for the geometry and boundary conditions of the model. An adaptive remeshing technique was implemented to address the potential mesh entanglement during the meshing process. Figure 1 illustrates the weldment geometry, governing equations, and boundary conditions for both homogeneous and heterogeneous welds, while Figure 2 shows the boundary conditions and adaptive meshing applied in COMSOL Multiphysics for both weld types.

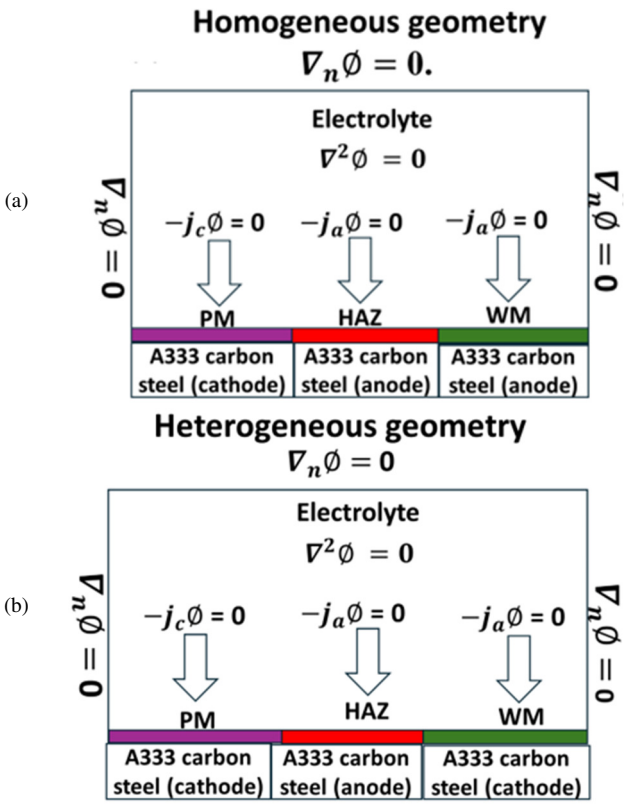

Fig. 1. Weldment geometry along with governing equation and boundary condition for: (a) homogeneous and (b) heterogeneous welds.

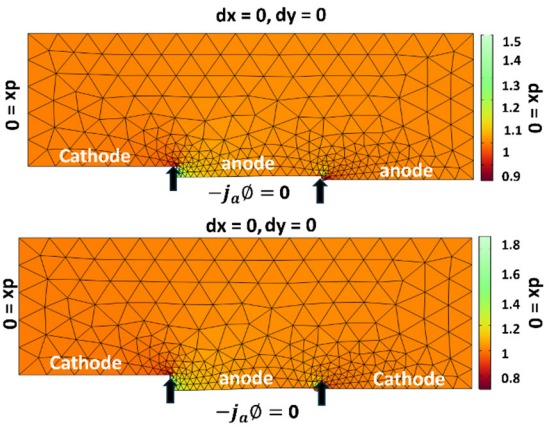

Fig. 2. Boundary conditions and adaptive meshing for ALE method to accurately predict corrosion in: (a) homogeneous and (b) heterogeneous welds.

III. RESULTS AND DISCUSSION

A. *Effect of Temperature on Corrosion Behavior*

Figure 3 presents the effect of temperature on the corrosion rate of PM, HAZ, and WM in 3 wt% NaCl solution. At 25 °C (Figures 3(a) and 3(b)), the homogeneous weld exhibited minimal galvanic corrosion, with the C_R values stabilizing at ± 3 mm/y, suggesting electrochemical homogeneity compared to the heterogeneous weld that showed a higher galvanic effect, with the WM reaching 4.5 mm/y, while the HAZ decreased to - 5 mm/y within the first 10 h. This indicates that WM behaved anodically while HAZ behaved cathodically. At 60 °C, as displayed in Figures 3(c-d), these trends were exacerbated in the heterogeneous weld, with the WM's corrosion rate reaching 6 mm/y, and HAZ increasing to 6.5 mm/y. This may be due to the enhanced galvanic polarization driven by ion mobility and reaction kinetics. In contrast, the homogeneous weld remained invariant, with corrosion rates within ± 5 mm/y. These observations aligned with the corrosion science principles, where galvanic couples between dissimilar zones of heterogeneous welds led to accelerated anodic dissolution of the less noble zones.

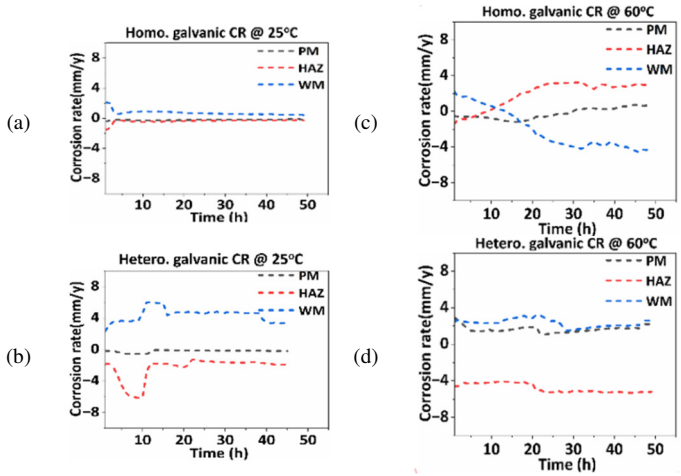

Fig. 3. Experimental galvanic C_R of PM, HAZ, and WM in 3 wt % NaCl (autogenous pH): (a)-(b) both welds at 25 °C, and (c)-(d) both welds at 60 °C.

B. *Galvanic Effects*

Figure 4 describes the average corrosion rate among PM, HAZ, and WM for both homogeneous and heterogeneous welds at 25 °C and 60 °C. At 25 °C (Figure 4(a)), PM in the homogeneous weld exhibited a lower corrosion rate of - 0.5 mm/y, compared to HAZ and WM, which had rates of - 2.0 mm/y and 2.97 mm/y, respectively. The PM's uniform microstructure reduces its susceptibility to corrosion, while the HAZ and WM experience galvanic effects due to differences in chemical composition and microstructure. WM presented anodic behavior due to $FeCO_3$ formation, while PM and HAZ behaved cathodically. In the heterogeneous weld, the behavior of both the PM and HAZ aligned with that of homogeneous weld, further illustrating the galvanic effects at lower temperatures. Conversely, in higher temperature (Figure 4(b)), the corrosion rates increased, with HAZ rising to - 4.32 mm/y, WM to 3.68 mm/y, and PM to -1.2 mm/y. Elevated temperature increases ion mobility and electrolyte conductivity, enhancing galvanic corrosion. The WM of the heterogeneous weld exhibited the highest corrosion rate at 2.92 mm/y due to the nickel-enriched filler metal, which makes it more anodic than the other two.

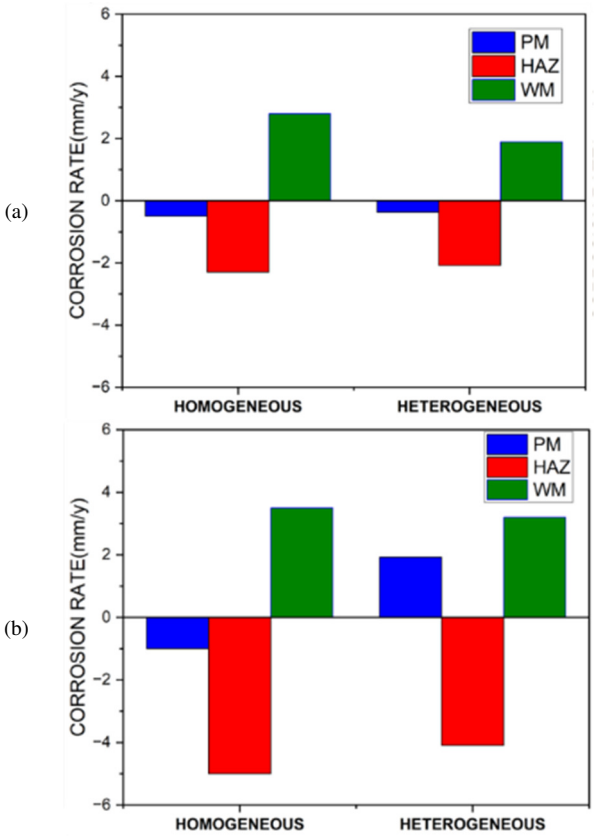

Fig. 4. Average galvanic C_R for PM, HAZ, PM comparing: (a) homogeneous weld and (b) heterogeneous weld at 3 wt % NaCl, 25 °C and 60 °C.

C. *Model Predictions*

The standardized Nernst-Planck equation was used to simulate the current density and potential distribution at the electrode-electrolyte interface. Figure 5 illustrates the

relationship between the electrode-electrolyte interface at 25 °C and 60 °C, confirming that the maximum metal loss occurred in the anodic regions (HAZ and WM), while PM remained cathodic. The electrolyte potential fluctuations were higher at the anodic surface at 60 °C, indicating greater current density compared to 25 °C due to increased ion dissolution and conductivity. Figure 6 depicts the simulated galvanic graphs of the corrosion rates at 25 °C and 60 °C. At 25 °C (Figures 6(a) and 6(b)), the WM of the homogeneous weld behaved anodically with a corrosion rate of 1.6 mm/y, while HAZ initially showed cathodic behavior at - 1.7 mm/y, before slightly increasing. In contrast, heterogeneous welds demonstrated a lower corrosion rate in the WM (2.6 mm/y) and consistently cathodic HAZ. This can be attributed to the similar electrochemical potential in homogeneous materials, leading to stronger galvanic interactions, especially from HAZ to WM. At 60 °C, corrosion intensified overall (Figures 6(c) and 6(d)). In homogeneous welds, HAZ became highly anodic (rising to 3.6 mm/y), while WM more cathodic (- 1.4 mm/y). For heterogeneous welds, WM behaved anodically with a corrosion rate of 3.6 mm/y, while HAZ remained cathodic. The stronger galvanic cell in heterogeneous joints resulted from dissimilar metal potential, particularly under heat, which makes the WM more susceptible to corrosion.

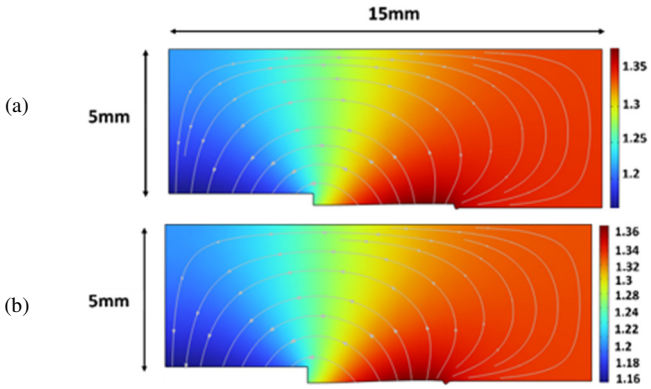

Fig. 5. Electrode potential distributions at: (a) 25 °C and (b) 60 °C.

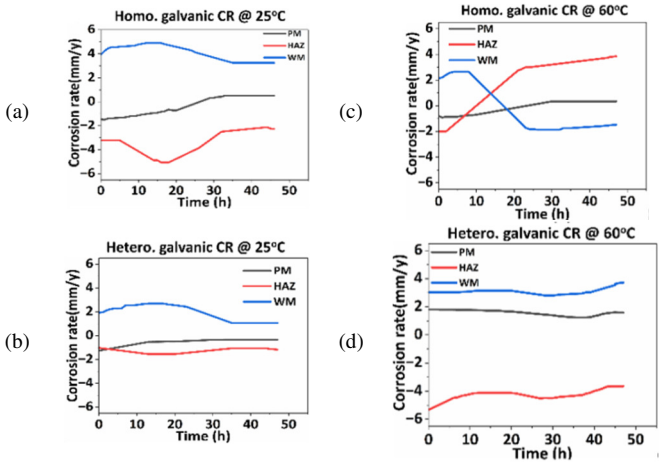

Fig. 6. Simulated galvanic corrosion rates for PM, HAZ, and WM: (a)-(b) both welds at 25 °C, and (c)-(d) both welds at 60 °C.

D. Model Validation and Result Comparison

The validation of the numerical model was carried out by comparing the experimental and simulated corrosion rates for both homogeneous and heterogeneous welds at 25 °C and 60 °C (Figure 7). The results showed that the simulated corrosion rates displayed similar trends to the experimental data, with deviations observed primarily in the initial stages of testing. These deviations can be attributed to variations in environmental conditions, such as temperature fluctuations, and potential differences in the electrolyte composition that the model could not fully account for. Despite these discrepancies, the general trends were consistent, highlighting the ability of the model to predict the corrosion behavior under varying conditions. Further validation using a parity plot (Figure 8) confirmed that the experimental and simulated corrosion rates were correlated within a ± 20% error margin, with some discrepancies. These deviations can be attributed to the complexities involved in modeling galvanic corrosion, especially considering the high activity of H^+ ions and local pH changes that occurred in real environments.

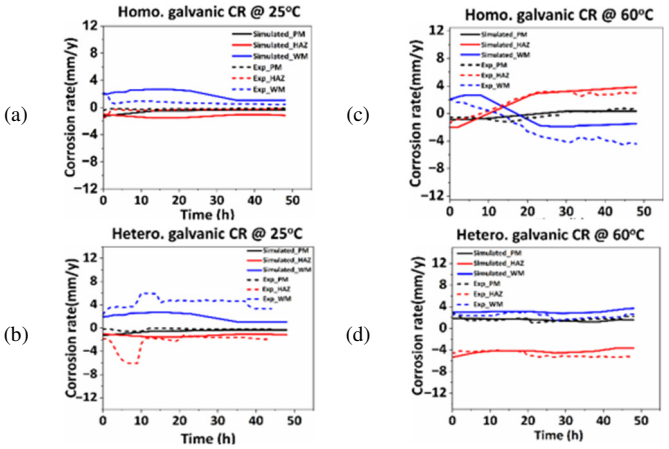

Fig. 7. Comparison of experimental and simulated galvanic corrosion rates for PM, HAZ, and WM at (a)-(b) 25 °C, and (c)-(d) 60 °C.

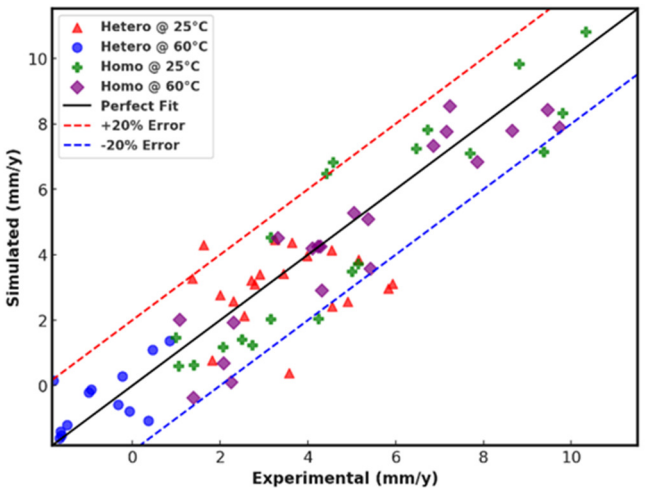

Fig. 8. Parity plot for both simulated and experimental results of galvanic C_R for PM, HAZ, and WM for both welds at 25 °C and 60 °C.

Figure 9 and Table IV further compared the experimental and simulated corrosion rates at 25 °C and 60 °C.

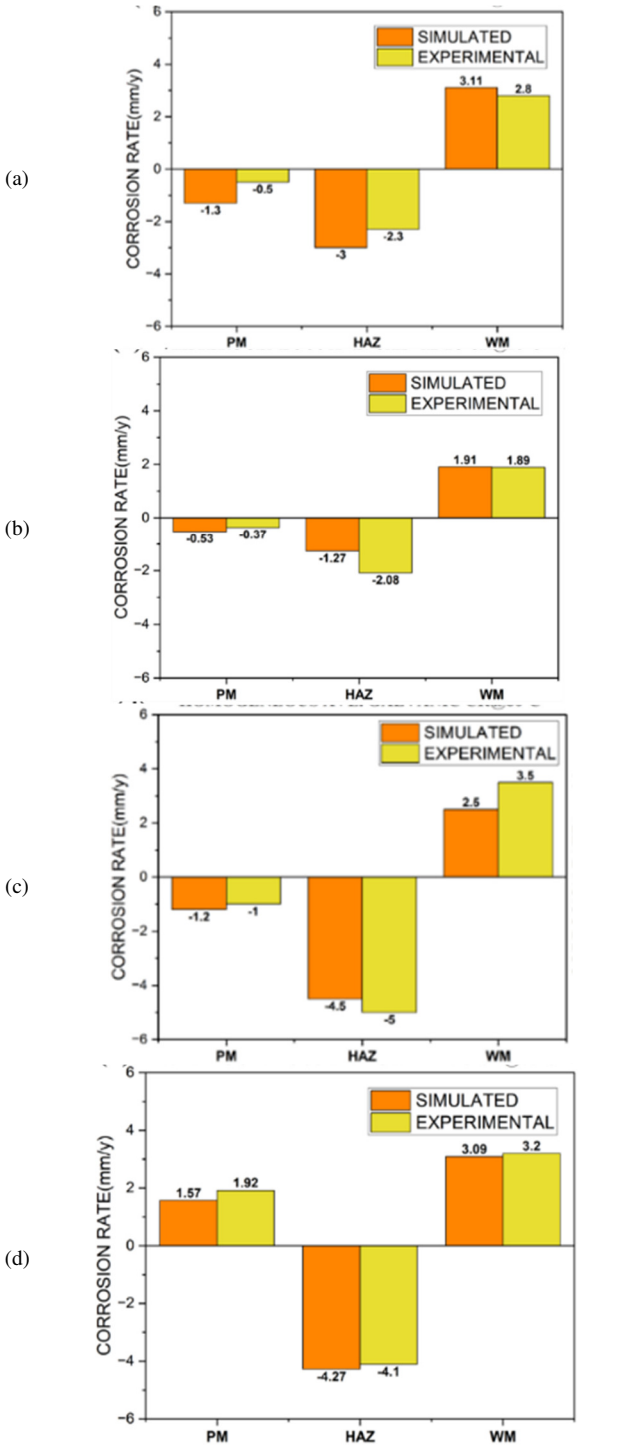

Fig. 9. Validation of the simulated and experimental galvanic C_R distribution of the PM, HAZ, and WM for both welds (a)-(b) at 25 °C, and (c)-(d) at 60 °C.

For the homogeneous weld at 25 °C, the WM corrosion rate ranged from 2.8 mm/y to 3.5 mm/y experimentally and from 3.1 mm/y to 3.6 mm/y in the simulations, showing good agreement. The PM zone exhibited a lower corrosion rate of 0.3 - 0.5 mm/y experimentally and 0.5 - 0.7 mm/y in simulations, consistent with the more stable microstructure of the PM. The HAZ of the heterogeneous weld exhibited the highest corrosion due to the variation in grain structure and phase distribution.

At 60 °C, the corrosion rates were higher, with the WM displaying the highest corrosion rate. The experimental values for WM ranged from 3.0 mm/y to 3.8 mm/y, while the simulation predicted values between 2.5 mm/y and 3.3mm/y. Similarly, the PM zone exhibited experimental and simulated corrosion rates of 0.8 - 1.0 mm/y and 1.0 - 1.2 mm/y. These results indicated that the model accurately emphasized the influence of temperature on corrosion rates.

TABLE IV. COMPARISON OF EXPERIMENTAL AND SIMULATED CORROSION RATES FOR THE WELDMENT

Temperature	Weldment zone	Average simulated C_R	Average experimental C_R	% error
Homogeneous				
25 °C	PM	-1.30	-1.10	18
	HAZ	-3.00	-2.30	34
	WM	3.11	2.80	11
60 °C	PM	-1.20	-1.00	19
	HAZ	-4.50	-5.00	-10
	WM	2.50	3.50	-29
Heterogeneous				
25 °C	PM	-0.53	-0.37	43
	HAZ	-1.27	-2.08	-39
	WM	1.91	1.89	1
60 °C	PM	1.57	1.92	-18
	HAZ	-4.27	-4.10	4
	WM	3.09	3.20	-3

IV. CONCLUSIONS

This study examined the galvanic corrosion behavior of A333 carbon steel weldments under CO_2-saturated conditions by combining experimental electrochemical techniques with computational simulations. The findings indicated that elevated temperatures exacerbated the galvanic corrosion due to the increased rate of corrosion activities, especially in the Heat-Affected Zone (HAZ) and Weld Metal (WM). In addition, the heterogeneous welds, with nickel-containing filler compositions, exhibited higher susceptibility to galvanic effects compared to the homogeneous welds, made with matching filler and base metal compositions. The observed results can be attributed to the increased formation of localized galvanic cells, driven by variations in weld microstructures and compositional differences. Both Zero-Resistance Ammeter (ZRA) test and COMSOL Multiphysics simulations showed good agreement, attested to the validity of the model developed in predicting the corrosion susceptibility of the weldment zones.

This study highlighted the novelty and significance of using COMSOL Multiphysics to successfully model the galvanic corrosion in weld joints, with validation through experimental work, an approach not widely adopted in earlier research.

ACKNOWLEDGEMENT

This work is supported by Universiti Teknologi PETRONAS through YUTP-FRG grant (015LC0-493).

REFERENCES

[1] A. I. Al-Mosawi and S. Abbas Abdulsada, "Efficacy of polymeric liners in preventing internal corrosion of oil pipelines: A review," *Journal of Thermoplastic Composite Materials*, vol. 0, no. 0, pp. 1–26, Apr. 2025, https://doi.org/10.1177/08927057251334471.

[2] D. Fonseca, M. R. Tagliari, W. C. Guaglianoni, S. M. Tamborim, and M. F. Borges, "Carbon Dioxide Corrosion Mechanisms: Historical Development and Key Parameters of CO2-H2O Systems," *International Journal of Corrosion*, vol. 2024, no. 1, 2024, Art. no. 5537767, https://doi.org/10.1155/2024/5537767.

[3] A. A. Alkhimenko, B. S. Ermakov, Ya. I. Evstratikova, O. V. Shvetsov, and P. N. Khomich, "The influence of welded joint microstructure on the corrosive properties of X70 steel," *Metallurgist*, vol. 68, no. 11, pp. 1667–1675, Apr. 2025, https://doi.org/10.1007/s11015-025-01880-0.

[4] Q. Qiao, G. Cheng, W. Wu, Y. Li, H. Huang, and Z. Wei, "Failure analysis of corrosion at an inhomogeneous welded joint in a natural gas gathering pipeline considering the combined action of multiple factors," *Engineering Failure Analysis*, vol. 64, pp. 126–143, June 2016, https://doi.org/10.1016/j.engfailanal.2016.02.015.

[5] X. Dou *et al.*, "Corrosion of welding reinforcement height under dynamic conditions," *Physics of Fluids*, vol. 36, no. 3, Mar. 2024, Art. no. 035169, https://doi.org/10.1063/5.0197066.

[6] Q. Qiao, G. Cheng, Y. Li, W. Wu, H. Hu, and H. Huang, "Corrosion failure analyses of an elbow and an elbow-to-pipe weld in a natural gas gathering pipeline," *Engineering Failure Analysis*, vol. 82, pp. 599–616, Dec. 2017, https://doi.org/10.1016/j.engfailanal.2017.04.016.

[7] Z. M. Gader, I. Q. Hazim, and M. S. Abed, "Study the Corrosion Behavior of Low Carbon Steel Weldments Immersed in Tap Water," *Al-Qadisiyah Journal for Engineering Sciences*, vol. 17, no. 2, pp. 165–177, June 2024, https://doi.org/10.30772/qjes.2024.149684.1233.

[8] L. Huang, B. Brown, and S. Nesic, "Investigation of Environmental Effects on Intrinsic and Galvanic Corrosion of Mild Steel Weldment in CO2 Environment," in *NACE International's Annual Conference and Exposition, CORROSION 2014*, San Antonio, TX, USA, Mar. 2014, https://doi.org/10.5006/C2014-4374.

[9] J. Song *et al.*, "Study on the local corrosion behaviour and mechanism of bogie steel welded joints," *Corrosion Science*, vol. 208, Nov. 2022, Art. no. 110709, https://doi.org/10.1016/j.corsci.2022.110709.

[10] S. L. Henke, R. S. C. Paredes, and A. R. Capra, "Development of delta ferrite on the weld and HAZ produced by pulsed plasma arc welding on a supermartensitic stainless steel," *Welding International*, vol. 29, no. 4, pp. 285–290, Apr. 2015, https://doi.org/10.1080/09507116.2014.932977.

[11] Y. Pu *et al.*, "Unlocking the effect of interfacial microstructure and *Desulfovibrio vulgaris* on corrosion characteristics in copper-nickel alloy welded joint," *Corrosion Science*, vol. 230, Apr. 2024, Art. no. 111947, https://doi.org/10.1016/j.corsci.2024.111947.

[12] E. V. Morales, A. Cruz-Crespo, J. A. Pozo-Morejón, J. V. M. Oria, L. S. Araujo, and I. S. Bott, "Microstructural characteristics of different heat-affected zones in welded joints of UNS S32304 duplex stainless steel using the GMAW process: analysis of the pitting corrosion resistance," *Corrosion Reviews*, vol. 42, no. 1, pp. 93–105, Jan. 2024, https://doi.org/10.1515/corrrev-2023-0061.

[13] A. Lazareva, J. Owen, S. Vargas, R. Barker, and A. Neville, "Investigation of the evolution of an iron carbonate layer and its effect on localized corrosion of X65 carbon steel in CO2 corrosion environments," *Corrosion Science*, vol. 192, Nov. 2021, Art. no. 109849, https://doi.org/10.1016/j.corsci.2021.109849.

[14] A. Matamoros-Veloza, R. Barker, S. Vargas, and A. Neville, "Mechanistic Insights of Dissolution and Mechanical Breakdown of FeCO3 Corrosion Films," *ACS Applied Materials & Interfaces*, vol. 13, no. 4, pp. 5741–5751, Jan. 2021, https://doi.org/10.1021/acsami.0c18976.

[15] A. Mohammed Nor, M. F. Suhor, A. Z. Abas, and S. Mat, "Effect of CO2/H2S on Corrosion Behavior of API 5L 65 Carbon Steel in High pCO2 Environments," in *Offshore Technology Conference-Asia*, Kuala Lumpur, Malaysia, Mar. 2014, https://doi.org/10.4043/24962-MS.

[16] F. Pessu *et al.*, "Localized and General Corrosion Characteristics of Carbon Steel in H2S Environments," in *NACE International Annual Conference, CORROSION 2019*, Nashville, TN, USA, Mar. 2019, https://doi.org/10.5006/C2019-12943.

[17] M. Saeedikhani, S. Wijesinghe, and D. J. Blackwood, "Moving boundary simulation and mechanistic studies of the electrochemical corrosion protection by a damaged zinc coating," *Corrosion Science*, vol. 163, Feb. 2020, Art. no. 108296, https://doi.org/10.1016/j.corsci.2019.108296.

[18] M. Nordsveen, S. Nesic, R. Nyborg, A. Stangeland, "A Mechanistic Model for Carbon Dioxide Corrosion of Mild Steel in the Presence of Protective Iron Carbonate Films-Part 1: Theory and Verification," *CORROSION*, vol. 59, no. 5, pp. 443-456, May 2003, https://doi.org/10.5006/1.3277576.